

See discussions, stats, and author profiles for this publication at: <https://www.researchgate.net/publication/263944719>

Synthesis, Structural Characterization, and Sensing Properties of Clickable Unsymmetrical 1,1'-Disubstituted Ferrocene-Triazole Derivatives

ARTICLE in ORGANOMETALLICS · FEBRUARY 2012

Impact Factor: 4.13 · DOI: 10.1021/om300093c

CITATIONS

27

READS

23

5 AUTHORS, INCLUDING:



Francisco Otón

University of Murcia

39 PUBLICATIONS 754 CITATIONS

[SEE PROFILE](#)



Arturo Espinosa

University of Murcia

128 PUBLICATIONS 2,326 CITATIONS

[SEE PROFILE](#)



Alberto Tárraga

University of Murcia

173 PUBLICATIONS 3,700 CITATIONS

[SEE PROFILE](#)



Pedro Molina

University of Murcia

502 PUBLICATIONS 7,767 CITATIONS

[SEE PROFILE](#)

Synthesis, Structural Characterization, and Sensing Properties of Clickable Unsymmetrical 1,1'-Disubstituted Ferrocene-Triazole Derivatives

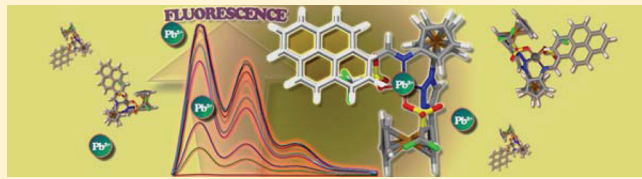
Francisco Otón,[†] María del Carmen González,[‡] Arturo Espinosa,[‡] Alberto Tárraga,^{*,‡} and Pedro Molina^{*,‡}

[†]Departamento de Nanociencia Molecular y Materiales Orgánicos, Instituto de Ciencia de Materiales de Barcelona (CSIC), Campus UAB, 08193 Bellaterra, Spain

[‡]Departamento de Química Orgánica, Facultad de Química Campus de Espinardo, Universidad de Murcia, E-30100 Murcia, Spain

Supporting Information

ABSTRACT: A variety of unsymmetrically 1,1'-disubstituted ferrocenes 3–5 have been prepared by using the tandem click reaction/Staudinger-azaWittig process and their cation complexation properties studied using electrochemical and spectroscopic techniques. The common structural features present in these ligands are the presence of another redox unit, connected to the 1-position of the central ferrocene core through a triazole ring, and a photoactive moiety linked to the 1'-position of such core through an imine group. Receptors 3 and 5 undergo perturbation of the CV in the presence of Pb^{2+} and Zn^{2+} cations, whereas receptor 4 undergoes a different type of perturbation in the presence of Ni^{2+} , Cd^{2+} , Zn^{2+} , and Pb^{2+} cations. The low-energy band of the absorption spectra of receptor 3 is blue-shifted, upon addition of Zn^{2+} , and Pb^{2+} cations, whereas receptor 4 in the presence of Ni^{2+} and Cd^{2+} undergoes a remarkable red shift ($\Delta\lambda = 110 \text{ nm}$) of the LE band which is responsible for the change of color from red to blue. Moreover, receptor 3 underwent a significant increase in its emission band in the presence of Pb^{2+} , whereas in receptor 5, such an increase is notably lower. In conclusion, receptor 4 behaves as a colorimetric receptor for Ni^{2+} and Cd^{2+} and 5 acts as a selective fluorescent receptor for the Pb^{2+} cation. On the basis of the ^1H NMR titration data and from the DFT theoretical calculations, tentative binding modes have been proposed for the metal complexes formed.



INTRODUCTION

Ferrocene derivatives in which the two cyclopentadienyl rings bear different substituents have attracted considerable interest, owing to their utility in the synthetic construction of large ferrocene-based assemblies.¹ Unsymmetrically 1,1'-disubstituted ferrocene derivatives can lead to improved multifunctional systems for molecular recognition processes. For instance, unsymmetrical 1,1'-disubstituted ferrocene derivatives with unique functional groups on each cyclopentadienyl (Cp) ring have been used to assemble electroactive peptide and DNA conjugates.² Thus, a different substituent at the other cyclopentadienyl ring can induce an intermolecular interaction or a change in the electrochemical parameters. Hence, reliable strategies for the synthesis of unsymmetrical ferrocene derivatives are certain to maintain broad utility in both fundamental and applied research.

Importantly, known synthetic methodologies for the preparation of unsymmetrically 1,1'-disubstituted ferrocene derivatives involve complex transformations.³ The methods of their preparation involve selective introduction of a second substituent in the 1'-position of a monosubstituted derivative or selective transformation of one substituent of symmetrically disubstituted compounds.

The ferrocene unit has largely proved to be a simple and remarkable redox-signaling unit. Thus, the preparation and sensing properties of ferrocene derivatives have been recently reviewed.⁴ In such ferrocene-containing ligands, cation binding at an adjacent receptor site induces a positive shift in the redox potential of the ferrocene/ferrocenium couple by through-space electrostatic communication, and the complexation ability of the ligand can be switched on and off by varying the applied electrochemical potential. The redox-active ferrocene moiety has also been exploited in the electrochemical sensing of anions; these receptors are expected to show cathodic shifts in their redox process when complexed to an anion, as they are easier to oxidize or harder to reduce than a free redox-active receptor.

In connection with our former studies on ferrocene derivatives as multichannel molecular sensors of anions and cations, we report in this paper the synthesis, structural characterization, and sensing properties of a new structural motif bearing a second ferrocene unit linked through a 1,2,3-triazole at one cyclopentadienyl ring, whereas the other unit is substituted by a fluorescent aromatic or heteroaromatic ring linked through an aldimine bridge. On this basis, suitable dual-signaling chemical

Received: February 6, 2012

Published: February 17, 2012



probes can be built by combining the redox activity of ferrocene, the photoactivity of the pyrene, fluorene, or quinoline, and the proven binding ability of the 1,2,3-triazole ring⁵ and the aldimine group.⁶

EXPERIMENTAL SECTION

General Comments. All reactions were carried out under N₂ using solvents which were dried by routine procedures. Commercial starting materials (aldehydes, ferrocene, *n*-butyllithium, and ethynylferrocene) were purchased from Aldrich and used without further purification. 1,1'-Bis(azido)ferrocene was prepared as described previously in the literature.⁷ Melting points were determined on a Kofler hot-plate melting point apparatus and are uncorrected. ¹H and ¹³C spectra were recorded on a Bruker 200, AC300, or 400 spectrometer. The following abbreviations for stating the multiplicity of the signals have been used: s (singlet), bs (broad singlet), d (doublet), st (pseudotriplet), m (multiplet), q (quaternary carbon). Chemical shifts refer to signals of tetramethylsilane in the case of ¹H and ¹³C spectra. The electron impact (EI) and electrospray (ESI) mass spectra were recorded on a Fisons AUTOSPEC 500 VG spectrometer. Microanalyses were performed on a Carlo Erba 1108 instrument. CV and OSWV techniques were performed with a conventional three-electrode configuration consisting of carbon working and platinum auxiliary electrodes and a Ag/AgCl reference electrode. The experiments were carried out with a 5 × 10⁻⁴ M solution of sample in CH₃CN or CH₂Cl₂ containing 0.1 M (*n*-C₄H₉)₄NPF₆ (TBAPF₆) as supporting electrolyte. All the potential values reported are relative to the ferrocene couple at room temperature. Deoxygenation of the solutions was achieved by bubbling nitrogen for at least 10 min, and the working electrode was cleaned after each run. The cyclic voltammograms were recorded with a scan rate increasing from 0.05 to 1.00 V s⁻¹, while the OSWV measurements were recorded at a scan rate of 100 mV s⁻¹ with a pulse height of 10 mV and a step time of 50 ms. Typically, the receptor (5 × 10⁻⁴ M) was dissolved in the appropriate solvent (5 mL) and TBAHP (base electrolyte) (0.194 g) added. The guest under investigation was then added as a 2.5 × 10⁻² M solution in the appropriate solvent using a microsyringe, while the cyclic voltammetric properties of the solution were monitored. Fc was used as an external and/or internal reference for both potential calibration and for reversibility criteria. Under similar conditions Fc has E = 0.39 V vs SCE and the anodic–cathodic peak separation is 67 mV. UV-vis and fluorescence spectra were carried out with the solvents and concentrations stated in the text and in the corresponding figure captions. Quantum yield values were measured with respect to anthracene as standard ($\Phi = 0.27 \pm 0.01$) using the equation $\Phi_x/\Phi_s = (S_x/S_s)[(1 - 10^{-A})/(1 - 10^{-A_s})] (n_s^2/n_x^2)^{1/2}$,⁸ where x and s indicate the unknown and standard solution, respectively, Φ is the quantum yield, S is the area under the emission curve, A is the absorbance at the excitation wavelength, and n is the refractive index.

Synthesis of 1-(4-Ferrocenyl-1,2,3-triazol-1-yl)-1'-azidoferrocene (1). 1,1'-Bis(azido)ferrocene⁷ (0.100 g, 0.37 mmol) and ethynylferrocene (0.078 g, 0.37 mmol) were dissolved in THF (15 mL) and mixed with a solution (3 mL) of hydrated copper sulfate (0.0046, 0.08 mmol) in distilled water. Then, a solution of sodium ascorbate (0.014 g, 0.08 mmol) in water (3 mL) was added and the mixture was stirred at room temperature for 8 h. Afterward, THF was removed under vacuum and the solid was filtered and washed with water (30 mL) and diethyl ether (30 mL). The solid was then dissolved in AcOEt/CH₂Cl₂ (1/19) and chromatographed in a silica gel column using this eluent ($R_f = 0.65$). The solid obtained was finally recrystallized in CH₂Cl₂/ethyl ether to give 0.073 g of 1 as a reddish brown solid (yield 41%). Mp: 231–234 °C dec. δ_{H} (200 MHz; CDCl₃; Me₄Si): 7.69 (s, 1H, CH), 4.98 (st, 2H), 4.77 (st, 2H), 4.38 (st, 2H), 4.32 (st, 2H), 4.29 (st, 2H), 4.13 (st, 2H), 4.11 (s, SH, Fc). δ_{C} (75 MHz; CD₂Cl₂): 147.0 (CH), 117.8 (CH), 101.5 (q), 94.7 (q), 75.0 (q), 69.6 (CH), 68.7 (CH), 67.6 (CH), 67.3 (CH), 66.7 (CH), 62.7 (CH), 62.2 (CH). ν_{max} (Nujol; cm⁻¹): 3088, 2111, 1688, 1291, 1226, 1159, 1134, 1105, 1067, 1038, 973, 879, 850, 819, 725. FAB⁺ MS (*m/z* (relative intensity)): 479 (M⁺ + 1, 98). Anal. Calcd for C₂₂H₁₈Fe₂N₆: C, 55.27; H, 3.79; N, 17.58. Found: C, 55.45; H, 4.03; N, 17.52.

General Procedure for the Synthesis of 1-(4-Ferrocenyl-1,2,3-triazol-1-yl)-1'-(methylene)aminoferrocene Derivatives 3–5. To a solution of 1 (120 mg, 0.25 mmol) in anhydrous THF (20 mL) was added a 1 M solution of trimethylphosphine (0.5 mL, 0.5 mmol) under nitrogen. Then, the reaction mixture was stirred at room temperature for 30 min, until the formation of the intermediate iminophosphorane 2 was completed. Afterward, a solution of the corresponding aldehyde (1 equiv) in the same solvent (30 mL) was added and the resulting reaction mixture was stirred overnight at room temperature. Then, the solvent was removed under vacuum and the residue obtained was triturated with ether and finally crystallized from *n*-Hex/AcOEt (1/1) to afford the pure products.

1-(4-Ferrocenyl-1,2,3-triazol-1-yl)-1'-(N-(pyren-1-yl)methylene)aminoferrocene (3). Yield: 70%. Mp: >250 °C. δ_{H} (400 MHz; CDCl₃; Me₄Si): 9.39 (s, 1H), 8.84 (d, 1H, ³J = 9.0 Hz), 8.51 (d, 1H, ³J = 8.4 Hz), 8.00–8.24 (m, 7H), 7.59 (s, 1H), 4.95 (bs, 2H), 4.77 (bs, 2H), 4.42 (bs, 2H), 4.35 (bs, 2H), 4.13 (bs, 2H), 3.84 (s, SH), 3.71 (bs, 2H). δ_{C} (100 MHz; CDCl₃): 157.1 (CH), 146.5 (q), 133.1 (q), 131.3 (q), 130.7 (q), 129.9 (q), 128.9 (CH), 128.6 (CH), 128.5 (q), 127.6 (CH), 126.3 (CH), 126.1 (CH), 125.9 (CH), 125.7 (CH), 125.2 (CH), 124.7 (q), 122.5 (CH), 117.9 (CH), 107.0 (q), 94.9 (q), 74.5 (q), 69.3 (CH), 69.3 (CH), 68.0 (CH), 67.7 (CH), 66.0 (CH), 64.8 (CH), 63.2 (CH). ν_{max} (CHCl₃; cm⁻¹): 3125, 3111, 2917, 2855, 1589, 1519, 1444, 1384, 1215, 1184, 1159, 1103, 1066, 1026, 879, 853, 842, 818. ESI MS (*m/z* (relative intensity)): 664 (M⁺, 100). Anal. Calcd for C₃₉H₂₈Fe₂N₄: C, 70.51; H, 4.25; N, 8.43. Found: C, 70.27; H, 4.43; N, 8.71.

1-(4-Ferrocenyl-1,2,3-triazol-1-yl)-1'-(N-(quinolin-2-yl)methylene)aminoferrocene (4). Yield: 75%. Mp: 235–238 °C dec. δ_{H} (300 MHz; CDCl₃; Me₄Si): 8.60 (s, 1H), 7.98 (m, 2H), 7.89 (d, 1H), 7.74 (m, 3H), 7.55 (m, 1H), 4.94 (bs, 2H), 4.74 (bs, 2H), 4.41 (bs, 2H), 4.37 (bs, 2H), 4.30 (bs, 2H), 4.03 (bs, 2H), 3.93 (s, SH). δ_{C} (75 MHz; CD₂Cl₂): 159.4 (CH), 155.1 (q), 148.3 (q), 146.6 (q), 136.5 (CH), 129.7 (CH), 129.5 (CH), 128.7 (q), 127.9 (CH), 127.2 (CH), 118.1 (CH), 117.8 (CH), 104.5 (q), 94.9 (q), 75.0 (q), 69.8 (CH), 69.4 (CH), 68.4 (CH), 67.9 (CH), 66.3 (CH), 65.2 (CH), 62.8 (CH). ν_{max} (CHCl₃; cm⁻¹): 3118, 3078, 2960, 2917, 2850, 1594, 1560, 1528, 1500, 1428, 1310, 1220, 1105, 1069, 1038, 952, 896, 881, 816. ESI MS (*m/z* (relative intensity)): 591.0 (M⁺, 100). Anal. Calcd for C₃₂H₂₅Fe₂N₅: C, 65.00; H, 4.26; N, 11.84. Found: C, 64.72; H, 4.08; N, 11.62.

1-(4-Ferrocenyl-1,2,3-triazol-1-yl)-1'-(N-(fluoren-2-yl)methylene)aminoferrocene (5). Yield: 60%. Mp: 234–238 °C. δ_{H} (300 MHz; CDCl₃; Me₄Si): 8.39 (s, 1H), 7.83 (s, 1H), 7.80 (d, 1H, ³J = 7.0 Hz), 7.71 (d, 1H, ³J = 7.8 Hz), 7.65 (m, 2H), 7.55 (d, 1H, ³J = 7.0 Hz), 7.37 (m, 2H), 4.91 (s, 2H), 4.63 (s, 2H), 4.46 (s, 2H), 4.39 (s, 2H), 4.31 (s, 2H), 4.03 (s, 2H), 3.97 (s, SH), 3.81 (s, 2H). δ_{C} (100 MHz; CDCl₃): 158.8 (CH), 146.3 (q), 144.3 (q), 143.9 (q), 143.5 (q), 140.9 (q), 134.5 (q), 127.7 (CH), 127.1 (CH), 126.6 (CH), 124.8 (CH), 123.8 (CH), 120.1 (CH), 119.8 (CH), 117.7 (CH), 105.9 (q), 94.5 (q), 74.6 (q), 69.1 (CH), 68.7 (CH), 68.1 (CH), 67.3 (CH), 66.1 (CH), 64.4 (CH), 62.7 (CH), 36.5 (CH). ν_{max} (CHCl₃; cm⁻¹): 3127, 3092, 2960, 1590, 1520, 1462, 1402, 1376, 1222, 1104, 1047, 1025, 999, 880, 816. ESI MS (*m/z* (relative intensity)): 629 (M⁺ + 1, 100). Anal. Calcd for C₃₆H₂₈Fe₂N₄: C, 68.82; H, 4.49; N, 8.92. Found: C, 69.05; H, 4.23; N, 8.80.

X-ray Structural Analysis. Suitable single crystals of 4 (from a 0.5 mg/mL solution in CH₃CN/CH₂Cl₂ (1/1)) were measured at 300(2) K in a Bruker SMART Apex CCD instrument using graphite-monochromated Mo K α radiation ($\lambda = 0.71073 \text{ \AA}$) from an X-ray tube. The measurements were made in the range 2.44–28.22° for θ . Full-sphere data collection was carried out with ψ and ω scans. Programs used: data collection, Smart version 5.631 (Bruker AXS 1997-02); data reduction, Saint+ version 6.36A (Bruker AXS 2001); absorption correction, SADABS⁹ version 2.10 (Bruker AXS 2001). Structure solution and refinement was done by using SHELXTL¹⁰ version 6.14 (Bruker AXS 2000–2003). The structure was solved by direct methods and refined by full-matrix least-squares methods on F^2 .

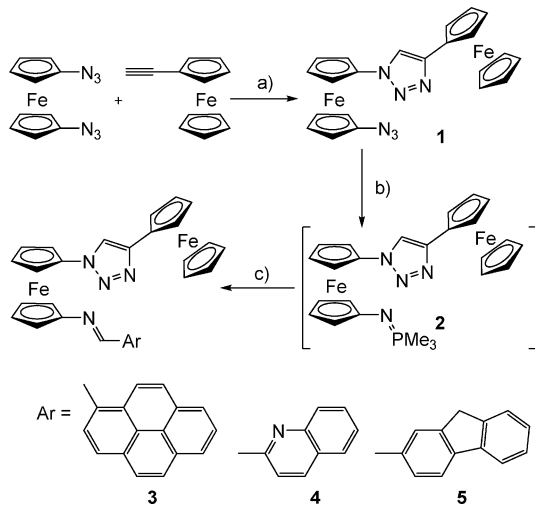
The non-hydrogen atoms were refined anisotropically. The H atoms were placed in geometrically optimized positions and forced to ride on the atom to which they are attached.

Computational Details. Quantum chemical calculations were performed with the ORCA electronic structure program package.¹¹ All geometry optimizations were run with tight convergence criteria, using the B3LYP¹² functional together with the new efficient RIJCOSX algorithm¹³ and the def2-TZVP basis set.¹⁴ In all optimizations a damped semiempirical correction accounting for the major part of the contribution of dispersion forces to the energy was included¹⁵ and denoted with the suffix D after the name of the functional (B3LYP-D). From these gas-phase optimized geometries all reported data were obtained by means of single-point (SP) calculations using the more polarized def2-TZVPP basis set.¹⁶ Reported energies are uncorrected for the zero-point vibrational term. Bond strengths were characterized by means of Wiberg's bond indices (WBI)¹⁷ and Mayer's bond orders (MBO).¹⁸ Also the electron density at bond critical points (BCPs), $\rho(r_c)$, derived from the topological analysis within the context of Bader's atoms-in-molecules methodology,¹⁹ was used as a bond strength descriptor and computed using the AIM2000 software²⁰ and wave functions (B3LYP/def2-TZVPP) generated with the Gaussian 09 software.²¹ Figures 8–10 were generated with VMD 1.8.7.²² Estimation of the root-mean-square distance (rmsd) between the computed and experimental structures of receptor 4 was achieved with Mercury CSD 2.4 (Build RC5).²³

RESULTS AND DISCUSSION

Synthesis. The synthetic procedures followed for the preparation of compounds 3–5 are summarized in Scheme 1. This

Scheme 1. Preparation of Receptors 3–5^a



^aConditions: (a) CuSO₄·SH₂O, Na ascorbate, THF/H₂O, room temperature; (b) PMe₃, anhydrous THF; (c) 1-formylpyrene (3), 2-formylquinoline (4), or 2-formylfluorene (5) in THF.

methodology requires, as a key intermediate, compound 1, which can be prepared starting from the 1,1'-bis(azido)ferrocene, previously synthesized in a two-step sequence: bis-lithiation of ferrocene and subsequent treatment with 2,4,6-triisopropylphenylsulfonyl azide (trisyl azide).⁷ The conversion of 1,1'-bis(azido)ferrocene into 1 was then achieved in a one-step process by monofunctionalization of one azide group of the starting material, by using the click reaction²⁴ with the appropriate amounts of ethynylferrocene and a copper(II) sulfate/sodium ascorbate mixture. Compound 1 was obtained in moderate yield (41%) due to the simultaneous formation of

the corresponding 1,1'-bis(triazolyl)ferrocene²⁵ derivative. However, this problem does not imply any serious inconvenience for this synthetic route, because both triazole derivatives formed can be easily separated by column chromatography. The intermediate compound 1 underwent a Staudinger reaction with trimethylphosphine under anhydrous conditions to give the iminophosphorane derivative 2, which was not able to be isolated. Subsequent aza-Wittig reaction of iminophosphorane 2 with the appropriate aldehyde provided the corresponding imines 3–5 in 70%, 75% and 60% yields, respectively.

The structures of compounds 1 and 3–5 have been confirmed by the usual techniques (¹H NMR, ¹³C NMR, FT-IR, MS, and elemental analysis). In addition, the structure of compound 4 was also confirmed by single-crystal X-ray diffraction (XRD) analysis.

Compound 4 crystallizes from CH₃CN/CH₂Cl₂ (1/1) as red prisms in the monoclinic space group Cc. Figure 1 shows the molecular structure of 4, and in Table 1 a summary of its crystallographic data is collected (see also Figure S5 in the Supporting Information).

In compound 4, both Cp rings are arranged in an eclipsed conformation (dihedral angles C1–centroidCp(1–5)–centroidCp(6–10)–C6 and C23–centroidCp(23–27)–centroidCp(28–32)–C32 are 3.05 and 0.38°, respectively) and have an almost parallel orientation with a tilt angle of 1.14° for the disubstituted unit and 2.14° for the monosubstituted unit. Regarding the substituent on the ferrocene moieties, the quinoline ring and imine group are nearly coplanar with the Cp ring, and they are connected with their N atoms in an anti-periplanar conformation (dihedral angle 179.13°). In the other branch of the molecule the Cp rings connected through the triazole ring are also almost coplanar and are slightly tilted (angle 8.60°). However, the triazole ring is clearly out of the plane with dihedral angles of 19.22 and 10.97° with respect to the corresponding Cp planes. This small distortion is caused by the repulsion between the neighboring protons of the triazole and the ferrocene and by a very weak hydrogen bond formed between a N group of triazole and a ferrocene proton of a different molecule (N···H distance 2.466 Å, N···H–C angle 166.24°). A distance of 3.486 Å between the monosubstituted Cp centroid and the plane formed by the quinoline ring indicates a slipped intramolecular face-to-face π–π interaction that is also observed between neighboring molecules. With regard to the crystal packing of 4, in addition to the aforementioned weak hydrogen bond and the π–π interaction, another close contact is found between the imine nitrogen atom and a ferrocene moiety, but the long distance (N···H distance 2.525 Å) and the angle found (perpendicular to the imine plane) discard the presence of a hydrogen bond. Molecules form a herringbone structure in the (2,0,−2) plane, in which two columns of almost perpendicular molecules grow along the *b* axis. In this plane, each ferrocene moiety is surrounded by two perpendicular ferrocenes and a quinoline unit of three different molecules. Therefore, all π–π stacking interactions are located in the *ab* plane, while the N···H close contacts are connecting different layers along the *c* axis (see the crystal packing in Figure S5).

The DFT calculated (see Computational Details) structure agrees nicely with the aforementioned experimental structure in both overall conformational preference and in bond lengths and angles (rmsd 0.2312 Å). The largest discrepancies between experimental and calculated structures (Table S1 and Figure S50, Supporting Information) deal with dihedral angles between the

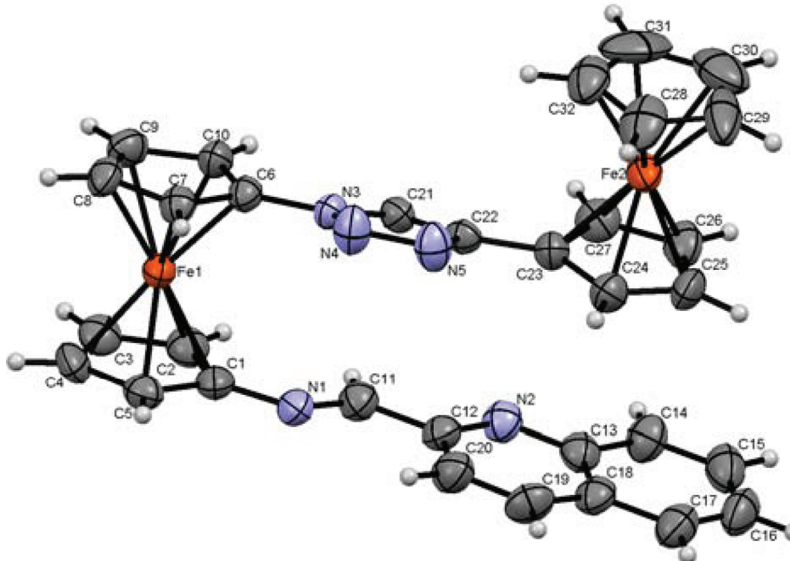


Figure 1. Molecular structure of **4** obtained by single-crystal XRD analysis. Thermal ellipsoids are drawn at the 50% probability level. Selected bond lengths (\AA) and angles (deg): Fe1–C1, 2.050(6); Fe1–C6, 2.034(6); Fe2–C32, 2.029(6); Fe2–C23, 2.051(6); N1–C11, 1.276(6); N1–C1, 1.426(7); N3–C6, 1.426(7); C22–C23, 1.474(7); C1–centroidCp(1–5)–centroidCp(6–10)–C6, 3.05; C23–centroidCp(23–27)–centroidCp(28–32)–C32, 0.38.

Table 1. Summary of Crystallographic Data for **4^a**

empirical formula	C ₃₂ H ₂₅ Fe ₂ N ₅	Z	4
formula wt	591.27	ρ_{calcd} (g cm ⁻³)	1.532
cryst syst	monoclinic	μ (mm ⁻¹)	1.165
space group	Cc	$2\theta_{\text{max}}$ (deg)	56.48
<i>a</i> (Å)	20.817(14)	no. of measd rflns	19 144
<i>b</i> (Å)	10.494(7)	no. of unique rflns	6189
<i>c</i> (Å)	11.911(8)	F_{000}	1216
α (deg)	90	R, R_w	0.0566, 0.1116
β (deg)	99.944(12)	R (all data)	R1 = 0.0902
γ (deg)	90	GOF	1.027
<i>V</i> (Å ³)	2563(3)	largest peak, hole (e Å ⁻³)	0.531, -0.268

^aCollected on a Bruker SMART Apex CCD instrument using Mo K α radiation ($\lambda = 0.7107 \text{ \AA}$) at 300(2) K.

triazole ring and the central ferrocene (N–N–C–Fe = -71.2° and -96.2° , respectively) or the outer ferrocene (N–N–C–Fe = -100.6° and -94.9° , respectively) and are imposed by the crystal packing. At the optimization level of theory, this global minimum energy conformer was found to be only 0.46 kcal/mol more stable than another stacked local minimum resulting from 180° rotation of the Fc–N(imine) single bond (and subsequent rotation along the inter-Cp-centroid axes at the central ferrocene).

Cation Binding Studies. The chemosensor behavior of **3–5** toward a variety of cations such as Li⁺, Na⁺, K⁺, Ca²⁺, Mg²⁺, Ni²⁺, Cd²⁺, Zn²⁺, Pb²⁺, Hg²⁺, and Cu²⁺ as perchlorate or triflate salts²⁶ was investigated by cyclic (CV) and Osteryoung square-wave (OSWV)²⁷ voltammetry as well as through spectrophotometric and ¹H NMR techniques. The spectrophotometric titration experiments were further analyzed using the computer program Specfit.²⁸

It is worth mentioning that while cyclic (CV) and Osteryoung square-wave (OSWV) voltammetry of compounds **3** and **5** were carried out in CH₃CN/CH₂Cl₂ (4/1, $c = 5 \times 10^{-4} \text{ M}$)

the voltamperograms of compound **4** should be obtained in CH₃CN/CH₂Cl₂ (3/2, $c = 5 \times 10^{-4} \text{ M}$) due to solubility problems. Under these conditions, each free receptor exhibited two reversible one-electron redox waves²⁹ at the half-wave potential values of $E^1_{1/2} = 0.05 \text{ V}$ and $E^2_{1/2} = 0.25 \text{ V}$ for **3** ($\Delta E_{1/2} = 0.02 \text{ V}$), at $E^1_{1/2} = 0.05 \text{ V}$ and $E^2_{1/2} = 0.31 \text{ V}$ for **4** ($\Delta E_{1/2} = 0.26 \text{ V}$), and at $E^1_{1/2} = 0.03 \text{ V}$ and $E^2_{1/2} = 0.24 \text{ V}$ for **5** ($\Delta E_{1/2} = 0.21 \text{ V}$), calculated versus the Fc⁺/Fc redox couple. The first oxidation wave corresponds to the monosubstituted ferrocene moiety and the second oxidation wave to the disubstituted moiety. This sequence can be inferred not only from the variation of the second redox potential upon changing the imine group when moving from **3** to **5** but also from the computed structures of the free receptors and the corresponding radical cations. We have reported³⁰ that the distance between the metal atom and the Cp ring centroid (Cp^o) has diagnostic relevance for characterizing the oxidation degree in metallocenes. Taking receptor **3** as an example, the corresponding oxidized species **3**⁺ shows an almost unaffected central disubstituted ferrocene ($\Delta d_{\text{Fe}-\text{Cp}^o} = -0.005$ and -0.002 \AA), whereas the outer monosubstituted unit displays the typical elongation ($\Delta d_{\text{Fe}-\text{Cp}^o} = 0.051$ and 0.058 \AA) observed in ferrocenium units. In OSWV two single-electron peaks also appear at the same potential as those obtained in the corresponding CV.

The results obtained on the stepwise addition of the aforementioned set of metal ions to electrochemical solutions of ligands **3–5** can be summarized as follows. (i) Only addition of Pb²⁺ and Zn²⁺ metal cations causes significant changes in the redox potentials of receptor **3** and **5**; in contrast, Ni²⁺, Cd²⁺, Zn²⁺, and Pb²⁺ are the cations which caused noticeable changes in the corresponding CV and OSWV of **4** upon their gradual addition to the free receptor. (ii) The electrochemical changes promoted by these metal cations are dependent on the type of ligand used: in the case of receptors **3** and **5**, the progressive addition of Pb²⁺ and Zn²⁺ induces a simultaneous anodic shift of the lower potential wave and a cathodic shift of the higher potential wave, thus appearing only a single wave in the voltammograms of

the final complex as a consequence of the superposition of the oxidation waves of both ferrocene units present in such receptors (Figure 2 and Table 2 and Figures S9, S14, and S15)

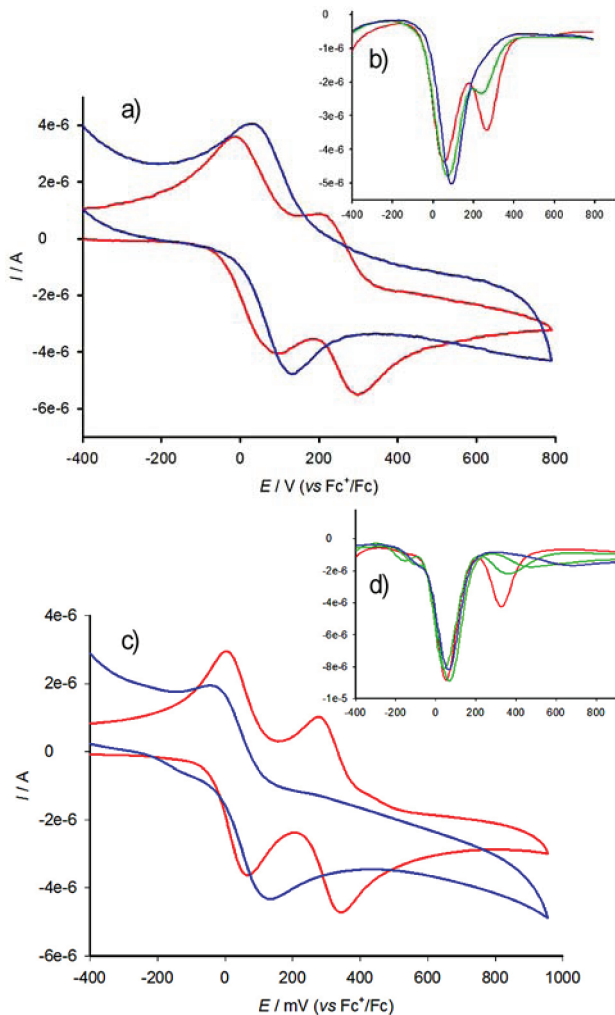
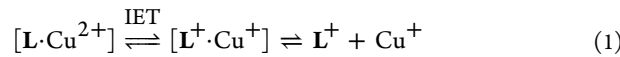


Figure 2. CV and OSWV of compound 3 (a, b) and 4 (c, d) ($c = 5 \times 10^{-4}$ M) in $\text{CH}_3\text{CN}/\text{CH}_2\text{Cl}_2$ (4/1) with $n\text{-Bu}_4\text{NPF}_6$ ($c = 0.1$ M), scanned at 0.1 V s $^{-1}$, upon addition of 3 equiv (ligand 3) or 4 equiv (ligand 4) of Pb^{2+} . Red lines correspond to the free ligand (3 or 4), and the blue lines result after addition of the Pb^{2+} metal cation.

(Supporting Information)). A remarkable difference between 3 and 5 is the lower affinity of 5 toward Zn^{2+} , attending to the higher amount of metal necessary to observe the electrochemical change: 4 equiv for 3 and 30 equiv for 5. In contrast, the most significant changes observed upon addition of Ni^{2+} , Cd^{2+} , Zn^{2+} , and Pb^{2+} to receptor 4 are produced in the higher oxidation wave of the free receptor, which undergoes a progressive anodic shift and also a simultaneous decrease in intensity until total disappearance, while the lower potential waves of the complexes formed appear at the same potential ($E_{1/2} = 0.05$ V) as that observed in the free receptor. These results seem to indicate that the triazole moiety interacts weakly in the complexation of the metal cations. Consequently, the binding process should be mainly located in the imine arm of the different receptors, especially in receptor 4 bearing an additional quinoline ring.

It is worth mentioning that addition of Cu^{2+} and Hg^{2+} metal cations induces the oxidation of these receptors as a consequence

of the already reported strong oxidant character of these metal cations in CH_3CN .³¹ Thus, LSV (linear sweep voltammetry) studies carried out upon addition of 3 equiv of Cu^{2+} to the CH_3CN electrochemical solutions of such receptors showed a significant shift of the sigmoidal voltammetric wave toward cathodic currents, indicating that this metal cation promotes the oxidation of the free receptors (Figure S17, Supporting Information). In contrast, if a complexation process was taking place, such a sigmoidal voltammetric wave would undergo a shift toward more positive potentials.^{31b,c} Moreover, studies about the formation of copper(II) complexes with nitrogen-donor ligands bearing ferrocenyl pendants have also demonstrated that upon addition of Cu^{2+} metal ion to the free ferrocenyl receptor L an initial fast formation of a $[\text{L}\cdot\text{Cu}^{2+}]$ complex should take place. However, it is suggested that, in a second step, a slower intramolecular electron–electron transfer process, between $\text{Fe}^{2+}\sim\text{Cu}^{2+}$ and $\text{Fe}^{3+}\sim\text{Cu}^{+}$ valence tautomers³² occurs, leading to the formation of a $[\text{L}^+\cdot\text{Cu}^+]$ complex which undergoes rapid decomposition to give the oxidized free ligand L^+ together with Cu^+ (eq 1).



One of the most important attributes of these receptors is the presence of a ferrocene moiety in proximity of the cation-binding nitrogen atoms. Previous studies on ferrocene-based ligands have shown that their characteristic low-energy (LE) bands in the absorption spectra are perturbed upon complexation.³³ Therefore, the metal recognition properties of receptors 3–5 toward the aforementioned set of metal cations were also evaluated by UV-vis spectroscopy in $\text{CH}_3\text{CN}/\text{CH}_2\text{Cl}_2$. The absorption spectrum of these receptors are characterized by a high-energy (HE) absorption band at λ 284, 317, and 336 nm for 3–5, respectively. In addition, two low-energy (LE) bands are also observed: one in the range of λ 317–380 nm ($\epsilon = 25\,500\text{--}10\,800 \text{ dm}^3 \text{ mol}^{-1} \text{ cm}^{-1}$) and another weaker band in the range of λ 479–495 nm ($\epsilon = 1500\text{--}2060 \text{ dm}^3 \text{ mol}^{-1} \text{ cm}^{-1}$), which is responsible for the red color of all receptors (Table 2). This band is assigned to a localized excitation with a lower energy produced by two nearly degenerate transitions, a Fe(II) d–d transition³⁴ or a metal-to-ligand charge transfer (MLCT) process ($d\pi\text{--}\pi^*$).³⁵

The optical detection capability of receptor 3 toward the aforementioned set of metal cations, upon addition of increasing amounts of such ions to a $\text{CH}_3\text{CN}/\text{CH}_2\text{Cl}_2$ (4/1) solution ($c = 2 \times 10^{-5}$ M) of this receptor, demonstrates that only the presence of Pb^{2+} (3 equiv) and Zn^{2+} (9 equiv) induces changes in its absorption spectrum (Figure 3). Therefore, a blue shift of the band at λ 382 nm to a new structured band centered at λ 347 nm ($\Delta\lambda = 35$ nm) and the disappearance of the band at λ 492 nm is observed upon stepwise addition of Pb^{2+} . These changes, which are similar to those found upon addition of Zn^{2+} , give to the solution a yellowish red color (Table 2). The presence of isosbestic points during the titration process ensures that only two colored species are present in solution. The Job plot carried out gives a ligand to metal stoichiometry of 1/1. Data were fitted with the aforementioned commercial program that gave us the association constant $K_a = 1.1 \times 10^4 \text{ M}^{-1}$ for Zn^{2+} and $K_a = 2.7 \times 10^4 \text{ M}^{-1}$ for Pb^{2+} (errors lower than 10%). The calculated detection limits (D_{lim})³⁶ were 2.3×10^{-5} M for Zn^{2+} and 7.2×10^{-6} M for Pb^{2+} .

Similar studies carried out using the receptor 4 in $\text{CH}_3\text{CN}/\text{CH}_2\text{Cl}_2$ (3/2) solution ($c = 2.5 \times 10^{-5}$ M) evidenced that only

Table 2. Electrochemical and UV–Vis Data of Receptors 3–5 in the Presence of Metal Cations

compd	$E_{1/2}^1$ ($\Delta E_{1/2}^1$) ^a	$E_{1/2}^2$ ($\Delta E_{1/2}^2$) ^b	λ_{\max} ($10^{-3}\varepsilon$) ^c	$\Delta\lambda^d$	IP ^e
3	0.05	0.25	228 (26.82), 284 (12.5), 382 (10.85), 406 (sh), 492 (1.50)		
[3·Pb] ²⁺	0.10 (0.05)	0.10 (-0.15)	227 (27.25), 240 (27.27), 272 (13.62), 276 (16.40), 334 (7.35), 347 (9.00), 365 (7.77), 386 (3.25), 393 (sh)	-99	259, 287, 313, 354
[3·Zn] ²⁺	0.11 (0.06)	0.11 (-0.14)	233 (23.47), 271 (12.30), 276 (14.62), 330 (6.62), 334 (8.60), 379 (5.62), 397 (4.76), 448 (1.30)	-44	248, 305, 350
4	0.05	0.31	258 (28.18), 317 (15.03), 485 (1.85)		
[4·Cd] ²⁺	0.05 (0)	0.37 (0.05)	259 (30.66), 359 (10.22), 598 (1.59)	113	351, 438, 532
[4·Ni] ²⁺	0.05 (0)	0.44 (0.13)	257 (27.82), 353 (10.76), 596 (1.46)	111	343, 437, 533
[4·Pb] ²⁺	0.05 (0)	0.46 (0.15)	280 (sh), 373 (4.01), 432 (sh)	-53	f
[4·Zn] ²⁺	0.05 (0)	0.45 (0.14)	275 (27.26), 434 (sh)	-51	f
5	0.03	0.24	276 (27.88), 336 (25.51), 479 (2.06)		
[5·Pb] ²⁺	0.07 (0.04)	0.08 (-0.16)	270 (35.82), 320 (sh), 400 (sh)	-79	f
[5·Zn] ²⁺	0.04 (0.01)	0.04 (-0.20)	276 (29.80), 334 (sh) 406 (3.15)	-73	305, 378, 429, 549

^aHalf-wave potentials in V of the lower potential wave and electrochemical shifting observed upon complexation. ^bHalf-wave potentials in V of the higher potential wave and electrochemical shifting observed upon addition of the corresponding metal cation. ^c λ_{\max} in nm, ε in $\text{dm}^3 \text{ mol}^{-1} \text{ cm}^{-1}$.

^dShifting in nm from the appropriate lower energy band in the complex and in the free receptor. ^eIsosbestic points in nm. ^fTwo sets of isosbestic points are found during the evolution of these titrations, depending on the amount of cation added.

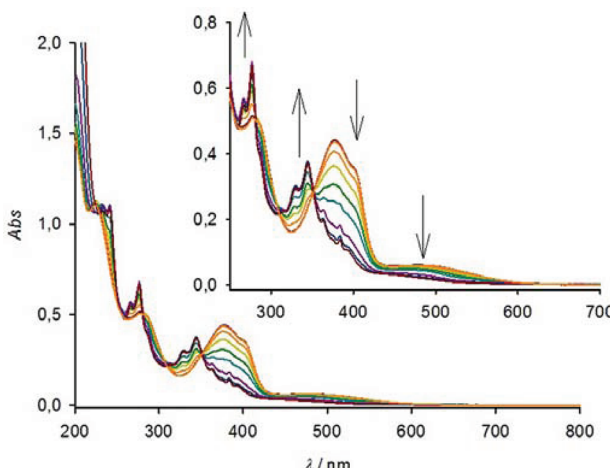


Figure 3. Changes in the UV–vis spectra of receptor 3 ($c = 2 \times 10^{-5} \text{ M}$) upon addition of increasing amount of Pb^{2+} (until 3 equiv) in $\text{CH}_3\text{CN}/\text{CH}_2\text{Cl}_2$ (4/1).

the presence of Ni^{2+} , Cd^{2+} , Zn^{2+} , and Pb^{2+} displayed modifications of the UV–vis spectrum of the free ligand, while the other metal cations did not generate any significant changes in the absorption spectrum of 4. However, the evolution of the UV–vis spectrum of the free ligand is dependent on the metal cation added. Thus, upon addition of Ni^{2+} and Cd^{2+} , large shifts of the LE band ($\Delta\lambda = 110 \text{ nm}$) bands were observed which gave rise to a change in the color of the solution from red to blue, making it evident that this receptor behaves as a “naked-eye” molecular sensor toward those cations (Figure S24). During the titration clear isosbestic points appear, indicating the presence of two species in the equilibrium (Table 2 and Figures S19 and S20). Job plot and titration profiles measured by UV–vis spectrophotometry indicated that receptor 4 binds Ni^{2+} and Cd^{2+} cations in a 2/1 (ligand/metal) fashion, the calculated global association constants being $\beta_2 = 1.4 \times 10^{10} \text{ M}^{-2}$ for Ni^{2+} and $\beta_2 = 4.8 \times 10^9 \text{ M}^{-2}$ for Cd^{2+} , while the calculated detection limits were $8.7 \times 10^{-7} \text{ M}$ for Ni^{2+} and $2.8 \times 10^{-6} \text{ M}$ for Cd^{2+} . However, addition of Zn^{2+} or Pb^{2+} causes two different tendencies in the UV–vis spectra (Figure 4 and

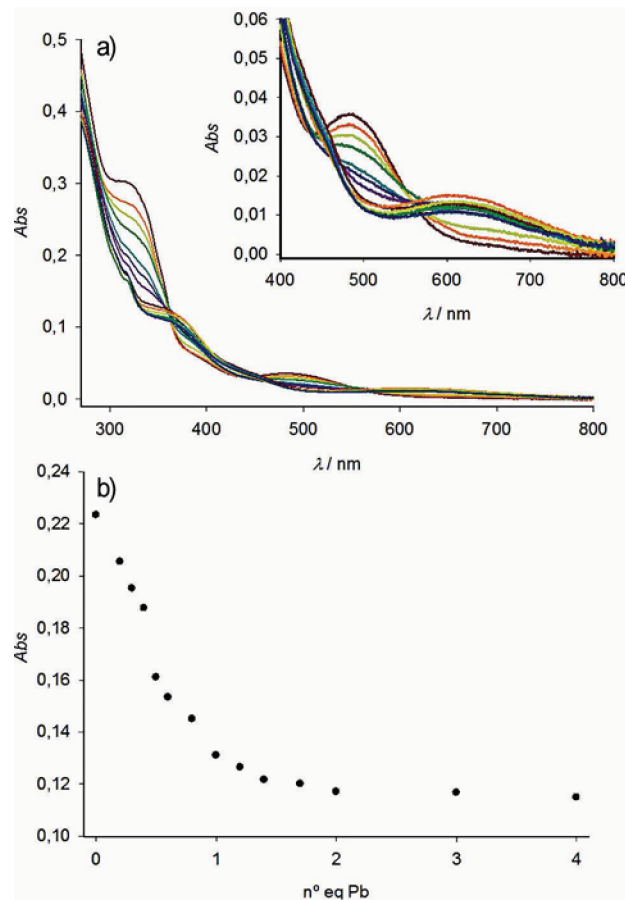


Figure 4. (a) Changes in the UV–vis spectra of receptor 4 ($c = 2.5 \times 10^{-5} \text{ M}$) in $\text{CH}_3\text{CN}/\text{CH}_2\text{Cl}_2$ (3/2) upon addition of 1.5 equiv of Pb^{2+} . (b) Binding profile at 380 nm upon addition of increasing amounts of Pb^{2+} .

Figure S21). At the beginning of the titration (upon addition of 0.3 equiv of the metal cations) the LE band undergoes red shifts similar to those observed for the case of Ni^{2+} and Cd^{2+} . However, the increase in the amount of cation added, until 1.3 equiv, promotes the simultaneous change of the UV–vis

spectra with the appearance of a new set of isosbestic points and a decrease in intensity or a blue shift of the low-energy bands, similarly to the receptor 3.

These facts seem to suggest that during the titration process two different complexes are formed depending on the amount of metal cation added. This final stage of the titration is similar to that found in receptor 3, with Pb^{2+} and Zn^{2+} denoting a 1/1 stoichiometry and the participation of both the imine–quinoline arm and the triazole moiety. As a Job plot cannot be used with confidence in these situations,³⁷ the titration profile and the fitting results were used to estimate the stoichiometry of the complexes formed by the Zn^{2+} and Pb^{2+} metal cations. The resulting data point to the initial formation of a complex with a 2/1 (ligand/metal) stoichiometry, similar to the case for the Cd^{2+} and Ni^{2+} complexes, which evolves to the final formation of a complex showing a 1/1 stoichiometry (Figure 3). By using the Specfit program, the association constants of these processes were estimated to be higher than $K_a > 10^6 \text{ M}^{-1}$ and $\beta_2 > 10^{12} \text{ M}^{-2}$. However, due to the characteristics of the titration and the high value of the estimated constants, we could not calculate reliable association constants.

The UV–vis study of receptor 5 gave results very similar to those observed for compound 3. The association constant with Zn^{2+} was calculated to be $K_a = 5.2 \times 10^3 \text{ M}^{-1}$, and the detection limits were $D_{\text{lim}} = 3.2 \times 10^{-6} \text{ M}$ for Pb^{2+} and $D_{\text{lim}} = 2.6 \times 10^{-6} \text{ M}$ for Zn^{2+} (other details are shown in Table 2 and in Figures S22 and S23). The association constant of the receptor with Pb^{2+} could not be calculated accurately, but data suggested the values are lower than those estimated for compound 3.

The oxidation experienced by these receptors in the presence of Cu^{2+} and Hg^{2+} has also been confirmed by UV–vis experiments. Thus, the electrochemical oxidation of these ligands was carried out at fixed potentials of 350 mV versus Fc^+/Fc , in order to achieve the oxidation of the two ferrocene moieties. This electrochemical oxidation was monitored by absorption spectroscopy, and the resulting spectrum shows a total agreement with those obtained upon addition of 3 equiv of Cu^{2+} or Hg^{2+} metal cations to the free receptors (Figure 5). In both cases, the appearance of a new band at 740 nm ($\epsilon = 720 \text{ M}^{-1} \text{ cm}^{-1}$) is observed which can be ascribed to the formation of a ferrocenium ion.^{32a–d}

Interestingly, the UV–visible–near-IR absorption spectra regularly recorded for different average number ($0 \leq n \leq 1$) of removed electrons show the appearance of a new weak and broad band, centered at 1040 nm. This band increases continuously in intensity until complete formation of the corresponding monooxidized ligand L^+ ($\text{L} = 3–5$) (Figure S25). However, the intensity of this band sequentially decreases until it disappears when the oxidation process continues until the dication L^{2+} is formed ($1 \leq n \leq 2$). This behavior is typical of an intervalence charge-transfer (IVCT) band due to the presence of an intramolecular electron-transfer process.³⁸ In summary, the presence of two ferrocene units in these ligands allows the electronic coupling between both redox units. The presence of the intervalence band also supports the electrochemical behavior of 3 and 5, in which the lack of electronic communication due to the metal complex formation should be responsible for the cathodic shift observed for the higher potential band of the free ligand upon addition of the corresponding metal cations.

The presence of fluorogenic moieties such as pyrene, quinoline, or fluorene in receptors 3–5 moved us to study their cation affinities by observing the extent to which their

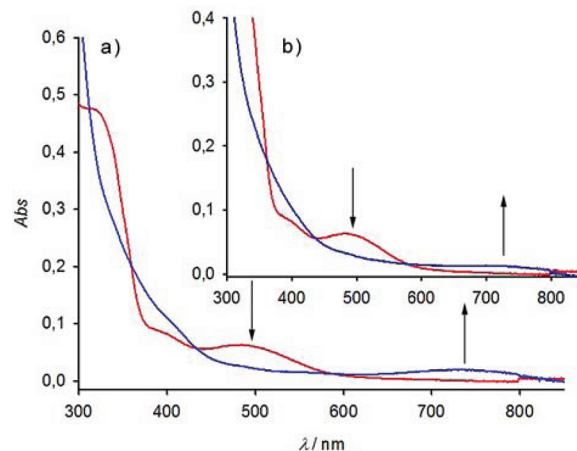


Figure 5. Evolution of the UV–vis spectra ($c = 2.5 \times 10^{-5} \text{ M}$) of 4 (red), in the region 300–800 nm, (a) upon addition up to 3 equiv of Cu^{2+} (blue line) and (b) upon its electrochemical oxidation (blue line). In both cases, the appearance of the same band indicating the formation of a ferrocenium ion is evident. Arrows indicate absorptions that increase or decrease during the experiment.

fluorescence intensities were affected in the presence of the aforementioned set of metal cations. As expected, when receptor 3 is excited at $\lambda_{\text{exc}} 350 \text{ nm}$, it exhibits a very weak fluorescence in $\text{CH}_3\text{CN}/\text{CH}_2\text{Cl}_2$ (4/1) solution ($c = 3.3 \times 10^{-6} \text{ M}$) ($\Phi_o < 0.001$) as a consequence of the quenching effect promoting by the triazole, imine, and ferrocene units present in its structure. Nevertheless, the emission bands ascribed to the monomeric emission of the pyrene unit are present in this spectrum. Fluorescence titration experiments demonstrate that only Pb^{2+} and Zn^{2+} caused a significant increase in the emission of the receptor, showing a large chelation-enhanced fluorescence factor (CHEF)³⁹ of 125 ($\Phi = 0.027$) for the case of Pb^{2+} and an importantly smaller CHEF = 17 ($\Phi = 0.004$) upon addition of Zn^{2+} (Figure 6). The stoichiometry of the complexes was also determined by the changes in the fluorogenic response of receptor 3 in the presence of varying concentrations of these metal cations, and the results indicate the

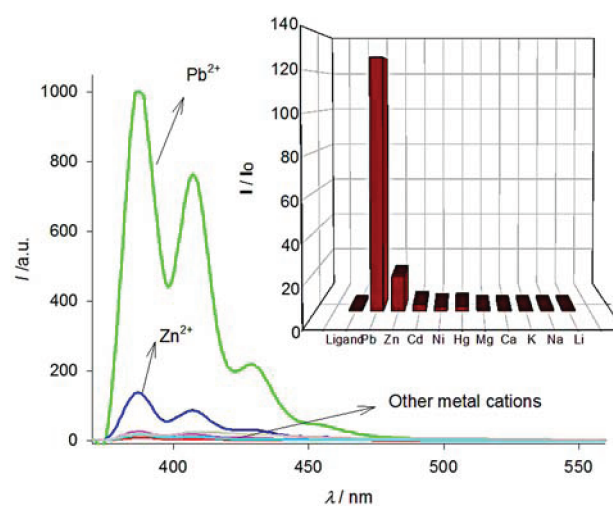


Figure 6. Fluorescent emission ($\lambda_{\text{exc}} 350 \text{ nm}$) of the free ligand 3 and the corresponding metal complexes $3-\text{M}^{n+}$ ($c = 3.3 \times 10^{-6} \text{ M}$) in $\text{CH}_3\text{CN}/\text{CH}_2\text{Cl}_2$ (4/1). The inset gives a bar diagram of the relative maximum intensities of the different species.

formation of 1/1 complexes. The calculated detection limits were found to be $D_{\text{lim}} = 5.9 \times 10^{-7}$ M for Pb^{2+} and $D_{\text{lim}} = 8.2 \times 10^{-7}$ M for Zn^{2+} . These small values show that this receptor is a very sensitive and selective fluorescent probe for the detection of Pb^{2+} .

The interference in the selective detection of Pb^{2+} , carried out in $\text{CH}_3\text{CN}/\text{CH}_2\text{Cl}_2$ (4/1) solution with receptor 3, from the other metal cations tested was also studied by using cross-selectivity experiments. Thus, addition of 10 equiv of Li^+ , Na^+ , K^+ , Ca^{2+} , Mg^{2+} , Cd^{2+} , or Ni^{2+} cation to 1 equiv of the receptor 3 in $\text{CH}_3\text{CN}/\text{CH}_2\text{Cl}_2$ (4/1) did not give any fluorescent response. However, further addition of 4 equiv of Pb^{2+} to the aforementioned solutions gave optical response identical with that observed upon addition of 4 equiv of Pb^{2+} to a solution containing only 1 equiv of the receptor 3 and which is free of the other metal cations (Figure S31). These results clearly demonstrate that this receptor has excellent affinity for Pb^{2+} over those ions.

On the other hand, emission of receptor 4 ($c = 5 \times 10^{-5}$ M) in $\text{CH}_3\text{CN}/\text{CH}_2\text{Cl}_2$ (3/2) is also scarcely observable ($\Phi_0 = 0.001$), when the sample is excited at $\lambda = 260$ nm. However, upon addition of the set of metal cations under study, only the presence of Zn^{2+} promotes a slight increase in the intensity of the emission band ($\text{CHEF} = 5$, $\Phi = 0.006$). In the case of 5, fluorescence emission of the free ligand ($c = 5 \times 10^{-6}$, $\lambda_{\text{exc}} = 276$ nm) is strongly quenched ($\Phi = 0.010$) and only Pb^{2+} and Zn^{2+} of all the cations tested caused changes in the emission spectrum. Addition of up to 16 equiv of Zn^{2+} caused a progressive increase of the fluorescence ($\text{CHEF} = 4$, $\Phi = 0.022$). In the case of Pb^{2+} when up to 2 equiv of the metal was added, an increase of fluorescence was observed ($\text{CHEF} = 6$, $\Phi = 0.036$) (Figures S30 and S32).

For the reported constant to be taken with confidence, we have proved the reversibility of the complexation process. Thus, once the appropriate complexes $[\text{L}\cdot\text{Me}^{2+}]$ ($\text{L} = 3-5$) were formed, their solutions were extracted several times with distilled water. The organic layer was dried, and the optical spectrum was recorded, and it was found to be the same as that of the free receptors. Afterward, the appropriate amounts of the adequate metal cations were added to these solutions and the initial UV-vis spectra of the corresponding metal complexes were fully recovered together. This experiment was carried out over several cycles, and the optical spectrum was recorded after each step, thus demonstrating the high degree of reversibility of the complexation/decomplexation process (Figures S27 and S28). It is necessary to mention here that a long exposure of the complexes to water causes the hydrolysis of the imine bond, although over a short period of time the presence of water does not damage the integrity of the receptors.

In order to gain insight into the coordination modes and into the nature of the complexes formed by these ligands upon addition of increasing amounts of the aforementioned cations, ^1H NMR titrations and ESI-MS experiments were also performed. CD_3CN was chosen as a solvent of the cations to afford a concentration suitable for ^1H NMR spectroscopic studies ($c = 2.5 \times 10^{-2}$ M). It is worth mentioning that the most common significant features of the free ligands are the presence of signals attributed to the $\text{CH}=\text{N}$ proton, those corresponding to the aromatic or heteroaromatic rings connected to the aldimine unit, six characteristic broad singlets corresponding to the H_α , $\text{H}_{\alpha'}$, $\text{H}_{\alpha''}$, H_β , $\text{H}_{\beta'}$, and $\text{H}_{\beta''}$ protons within the mono- and disubstituted cyclopentadienyl (Cp) units present in both ferrocene moieties, and a singlet assigned to the

protons of the unsubstituted Cp ring present in these molecules. Assignment of the ferrocene peaks in the free ligand has been done with the help of two-dimensional spectra and theoretical calculations (Figures S37, S38, and S41).

It is worth noting that ^1H NMR signals of receptor 3 ($\text{CD}_3\text{CN}/\text{CD}_2\text{Cl}_2$ 1/1) do not show any important shifting upon addition of increasing amounts of Zn^{2+} or Pb^{2+} ($\Delta\delta < 0.1$ ppm), although some ferrocene signals tend to split into two signals, increasing the number of signals, which makes very difficult the assignment of the signals in the complex. Moreover, the titration experiments could not be completed due to the insolubility of the complexes formed in any mixture of $\text{CD}_3\text{CN}/\text{CD}_2\text{Cl}_2$.

In the case of 4 (Figure 7), progressive addition of 1 or 2 equiv of metal cations induce a downfield shift not only of the

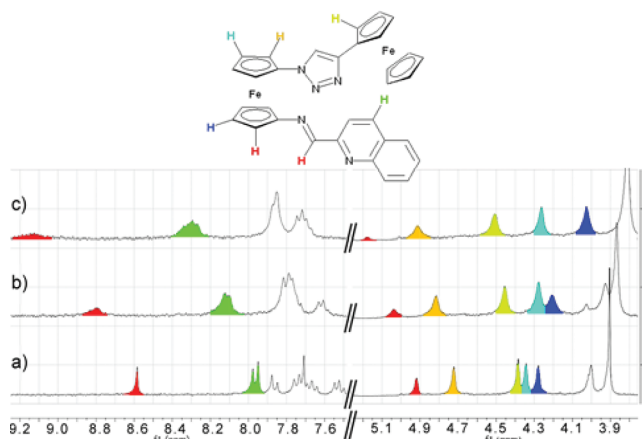
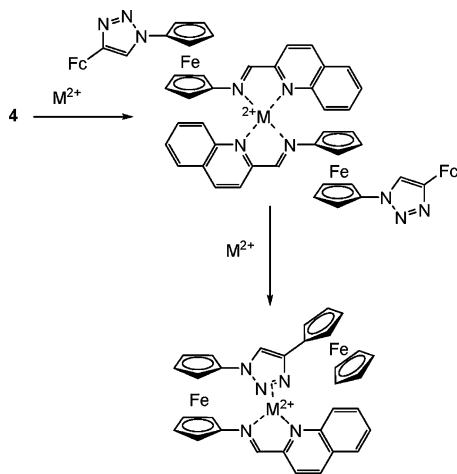


Figure 7. ^1H NMR titration of 4 in $\text{CD}_3\text{CN}/\text{CD}_2\text{Cl}_2$ (1/4) with (a) 0 equiv, (b) 0.5 equiv, and (d) 1 equiv of Pb^{2+} .

$\text{CH}=\text{N}$ proton but also of some protons of the quinoline ring. Ferrocene signals are also shifted downfield from their original positions, although to a lesser extent ($\Delta\delta < 0.15$ ppm). In general, we observed that during the complexation process the H_α protons of the two ferrocene units are shifted downfield while the H_β protons and those corresponding to the unsubstituted Cp ring do not move or are slightly shifted upfield. These facts could be attributed to the strong interaction between the N atoms present in the imine group and in the quinoline ring with formation of the corresponding bidentate chelate.

Moreover, taking also into account the 2/1 (ligand/metal) stoichiometry found from the UV-vis titration studies, we can in principle propose a tentative binding mode in which the imine-quinoline groups of two molecules of the receptor coordinate to the metal cations. Unfortunately, the NMR experiments do not give unambiguous information about the role of the triazole moiety in the coordination mode, but it is possible that in the 2/1 (L/M) complexes, previously formed during the titration experiments, they act only as mere spectators. However, once the 1/1 stoichiometry is reached, it could be possible that coordination through the triazole ring could take place, filling the coordination vacancies originated by the formation of the 1/1 complex (Scheme 2). In the case of Ni^{2+} the ^1H NMR signals totally vanished, which could be explained by the formation of a paramagnetic complex.

Scheme 2. Tentative Binding Modes Explaining the Evolution of the Stoichiometries Observed for the Complexes Derived from **4** upon Addition of Pb^{2+} and Zn^{2+} Metal Cations



The same type of titrations carried out in compound **5** show again a behavior similar to that shown by compound **3**. Therefore, addition of Pb^{2+} produces a small shielding of the imine proton and the ferrocene H_β and the unsubstituted Cp peaks of the terminal ferrocene, while the signal corresponding to the H_α protons of the central 1,1'-disubstituted ferrocene are slightly deshielded (Figures S39 and S40).

The stoichiometries proposed for the complexes formed by receptors **3–5** with Zn^{2+} and Pb^{2+} metal cations were further confirmed by electrospray mass spectrometry (ESI-MS) (Figures S42–S48). The measurements show the peaks at an m/z value corresponding to the complex $[\text{L}\cdot\text{M}^{2+}]$ ($\text{L} = \text{3–5}$) containing a ClO_4^- anion in the coordination sphere of the complexed metal cation: m/z 828 for $[\text{3}\cdot\text{ZnClO}_4]^\pm$, m/z 754 for $[\text{4}\cdot\text{ZnClO}_4]^\pm$, and m/z 793 for $[\text{5}\cdot\text{ZnClO}_4]^\pm$. In all cases, the relative abundance of their isotopic clusters was in good agreement with the simulated spectrum of such complexes. Interestingly, the ESI-MS spectrum of the $[\text{3}\cdot\text{Pb}^{2+}]$ complex shows a peak at m/z 871, indicating also the formation of the 1/1 complex bonded to three CH_3CN molecules. It is worth mentioning that in the ESI-MS spectra of receptor **4** in the presence of Ni^{2+} and Cd^{2+} metal cations only the fragments corresponding to the 1/1 complexes were detected: m/z 803 for $[\text{4}\cdot\text{CdClO}_4]^\pm$ and m/z 747 for $[\text{4}\cdot\text{NiClO}_4]^\pm$. It is worth noting that the relative abundance of the isotopic cluster for the complexes formed was in good agreement with the simulated spectrum in every case (Figure S49).

Binding of the aforementioned cations by receptors **3** and **4** has also been studied by DFT calculations. When compound **3** is used as the receptor, the presence of N donor atoms located at both side arms of the central disubstituted ferrocene hinge (Fc1) enables easy chelation of the metal cation. For the sake of simplicity we have used Zn^{2+} as a model for the complexation studies in the series of divalent cations, as it allows the use of all-electron basis sets. The minimum-energy structure for the resulting $3\cdot\text{Zn}(\text{OTf})_2$ complex (Figure 8) features the Zn atom in an almost perfectly tetrahedral environment of two N donor atoms, belonging to the imine ($d_{\text{N-Zn}} = 2.041 \text{ \AA}$; $\rho(r_c) = 8.09 \times 10^{-2} \text{ e/a}_0^3$; WBI 0.207; MBO 0.582) and triazole units ($d_{\text{N-Zn}} = 2.051 \text{ \AA}$; $\rho(r_c) = 7.58 \times 10^{-2} \text{ e/a}_0^3$; WBI 0.220; MBO 0.450), and two triflate O atoms ($d_{\text{O-Zn}} = 1.950$ and 1.994 \AA ;

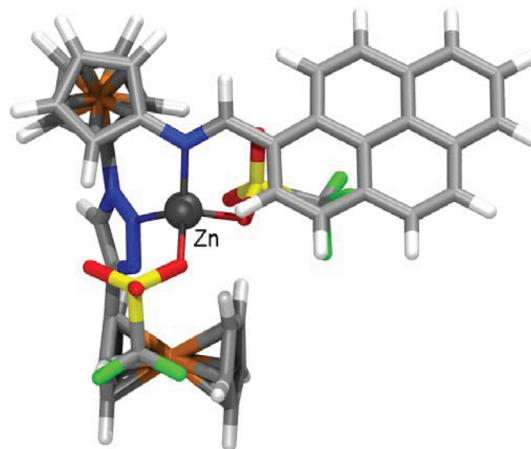


Figure 8. Calculated (B3LYP-D/def2-TZVP) minimum-energy structure for complex $3\cdot\text{Zn}(\text{OTf})_2$.

$\rho(r_c) = 8.42 \times 10^{-2}$ and $7.54 \times 10^{-2} \text{ e/a}_0^3$; WBI 0.214 and 0.199; MBO 0.500 and 0.380.

The analogous $3\cdot\text{Pb}(\text{ClO}_4)_2$ complex was also computed at a slightly lower computational level (using the less extensive def2-SVP)⁴⁰ basis set and shows, as the main geometric differential feature, the *hemidirected* environment around the metal due to the existence of the stereochemical electron pair, characteristic of $\text{Pb}(\text{II})$ ⁴¹ and other species, pointing outward in relation to the inner ferrocene hinge (Figure 9).

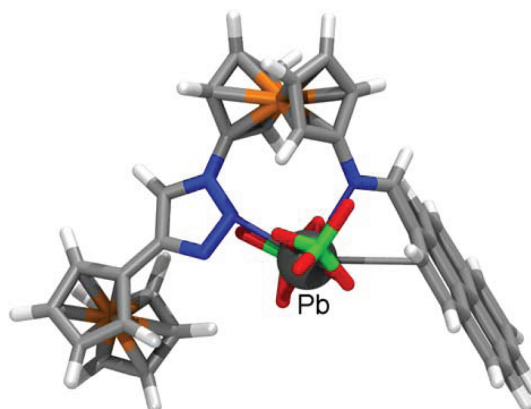


Figure 9. Calculated (B3LYP-D/def2-SVP) minimum-energy structure for complex $3\cdot\text{Pb}(\text{ClO}_4)_2$.

In contrast, ligand **4** features the quinoline–carbaldimine moiety that has a high ability for chelate formation.⁶ When the receptor is in excess (e.g. on addition of the divalent cation to a solution of the receptor), a $[4_2\cdot\text{M}]^{2+}$ stoichiometry seems to be favored. Nevertheless, when the ligand and metal cation are present in comparable amounts, a 1/1 (ligand/metal) complex is believed to be formed. The computed most stable structure for such a complex, in the case of the model Zn^{2+} cation (Figure 10), shows a trigonal-bipyramidal environment around the metal atom with the distal positions occupied by both heterocyclic N donor atoms ($d_{\text{N-Zn}} = 2.160$ and 2.212 \AA ; $\rho(r_c) = 6.20 \times 10^{-2}$ and $5.17 \times 10^{-2} \text{ e/a}_0^3$; WBI 0.157 and 0.175; MBO 0.408 and 0.163) almost aligned ($\text{N-Zn-N} = 166.4^\circ$). The imine N atom is more strongly bound at one of the equatorial positions ($d_{\text{N-Zn}} = 2.109 \text{ \AA}$; $\rho(r_c) = 6.92 \times 10^{-2} \text{ e/a}_0^3$; WBI 0.167; MBO 0.529), the other two being

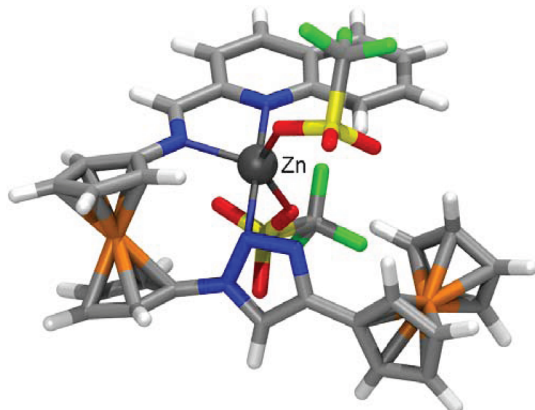


Figure 10. Calculated (B3LYP-D/def2-TZVP) minimum-energy structure for complex 4-Zn(OTf)_2 .

occupied by two O donor atoms ($d_{\text{O-Zn}} = 1.976$ and 2.071 \AA ; $\rho(r_c) = 7.81 \times 10^{-2}$ and $6.25 \times 10^{-2} \text{ e/a}_0^3$; WBI 0.209 and 0.181; MBO 0.460 and 0.305) belonging to triflate ligands.

The corresponding complexes of **4** with Pb^{2+} and Cd^{2+} were also computed at the lower B3LYP-D/def2-SVP computational level. In the case of $4\text{-Pb(ClO}_4)_2$, the overall structure (Supporting Information) very much resembles that of the corresponding Zn^{2+} complex shown in Figure 10. On the other hand, the Cd^{2+} cation prefers a 2/1 ligand/metal stoichiometry, as shown by the experimental data. The resulting complex does not show any remarkable ligand strain but is somehow crowded around the metal center. The latter adopts a distorted-octahedral environment owing to the difficulty of achieving a coplanar arrangement of the three N donor atoms—the pyridyl, imino, and triazolyl ones—belonging to every ligand (Supporting Information).

CONCLUSIONS

Three different unsymmetrically 1,1'-disubstituted ferrocenes linked to a 4-ferrocenyl-1,2,3-triazol-1-yl unit and to a functionalized imine group have been synthesized and studied as receptors for different metal cations through electrochemical and spectroscopic measurements. As a common electrochemical feature, these receptors display two reversible one-electron redox waves. Addition of Pb^{2+} and Zn^{2+} metal cations to receptors **3** and **5** induced an anodic shift of the wave associated with the oxidation of the monosubstituted ferrocene moiety and a cathodic shift of the 1,1'-disubstituted ferrocene unit. However, addition of Ni^{2+} , Cd^{2+} , Zn^{2+} , and Pb^{2+} cations to receptor **4** produced a gradual anodic shift of the oxidation wave assigned to the 1,1'-disubstituted ferrocene unit with concomitant decrease of its intensity, until total disappearance, while the lower potential waves, associated with the mono-substituted ferrocene moiety, appear at the same potentials as those observed in the free receptor. The different electrochemical behavior observed seems to indicate that different binding sites are concerned in the complexation processes. Thus, in receptors **3** and **5** the complexation should take place through the imine and triazole units present at the 1,1'-positions of the central ferrocene core. However, in the case of receptor **4** the main binding sites involved in the complexation should be the imine group of the receptor and the N atom of the quinoline ring, while the triazole unit only interacts very weakly with the metal cation.

On the other hand, a UV-vis study also demonstrates that receptors **3** and **5** act as appropriate receptors for Zn^{2+} and Pb^{2+} metal cations: the low-energy band is blue-shifted, which promotes the development of a yellowish-red color in the solution. Receptor **4** acts as a colorimetric molecular sensor for Ni^{2+} and Cd^{2+} : the low-energy band is red-shifted, which is responsible for the change of color from red to blue, making evident that this receptor behaves as a “naked-eye” molecular sensor toward those cations. Fluorescence studies showed that receptor **3** underwent a significant increase in the emission band of the receptor upon addition of Pb^{2+} and Zn^{2+} metal cations, whereas in receptor **5**, such an increase is notably lower.

In summary, receptor **3** could be considered a valuable receptor to selectively detect Pb^{2+} metal cations through three different channels, electrochemical, colorimetric, and fluorescent, while receptor **4** behaves as a colorimetric molecular sensor for Ni^{2+} and Cd^{2+} and receptor **5** acts as a selective fluorescent receptor for Pb^{2+} .

ASSOCIATED CONTENT

S Supporting Information

Figures and tables giving NMR spectra, electrochemical, UV-vis, emission, and ^1H NMR titration data, ESI-MS spectra, computational data, and energies and Cartesian coordinates for all computed species. This material is available free of charge via the Internet at <http://pubs.acs.org>.

AUTHOR INFORMATION

Corresponding Author

*E-mail: pmolina@um.es (P.M.); atarraga@um.es (A.T.).

Notes

The authors declare no competing financial interest.

ACKNOWLEDGMENTS

We gratefully acknowledge financial support from the MICINN-Spain, Project CTQ 2011/27175, and Fundación Séneca (Agencia de Ciencia y Tecnología de la Región de Murcia), project 04509/GERM/06 (Programa de Ayudas a Grupos de Excelencia de la Región de Murcia, Plan Regional de Ciencia y Tecnología 2007/2010). We also thank the Supercomputation Center at “Fundación Parque Científico de Murcia” (FPCMur) for technical support and the computational resources used in the supercomputer Ben-Arabi, and the Consejo Superior de Investigaciones Científicas (CSIC) of Spain for the award of a license for the use of the Cambridge Crystallographic Data Base (CSD). F.O. also acknowledges a Juan de la Cierva Postdoctoral Fellowship from MICINN.

REFERENCES

- (a) Seyferth, D.; Withers, H. P. Jr. *Organometallics* **1982**, *1*, 1275–1282. (b) Wright, M. E. *Organometallics* **1990**, *9*, 853–856. (c) Lai, L.-L.; Dong, T.-Y. *J. Chem. Soc., Chem. Commun.* **1994**, 2347–2348. (d) Iftime, G.; Moreau-Bossuet, C.; Manoury, E.; Balavoine, G. G. A. *J. Chem. Soc., Chem. Commun.* **1996**, 527–528. (e) Dong, T.-Y.; Lai, L.-L. *J. Organomet. Chem.* **1996**, *509*, 131–134. (f) Grossel, M. C.; Hamilton, D. G.; Vine, T. A. *Tetrahedron Lett.* **1997**, *38*, 4639–4642. (g) Xu, Y.; Kraatz, H. B. *Tetrahedron Lett.* **2001**, *42*, 2601–2603. (h) Rodríguez, J. G.; Pleite, S. J. *Organomet. Chem.* **2001**, 637–639, 230–239. (i) Chiffre, J.; Averseng, F.; Balavoine, G. G. A.; Daran, J. C.; Iftime, G.; Lacroix, P. G.; Manoury, E.; Nakatani, K. *Eur. J. Inorg. Chem.* **2001**, 2221–2226.
- (2) (a) Yu, C. J.; Wan, Y.; Yowanto, H.; Li, J.; Tao, C.; James, M. D.; Tan, C. L.; Blackburn, G. F.; Meade, T. J. *J. Am. Chem. Soc.* **2001**, *123*,

- 11155–11161. (b) Song, H.; Kerman, K.; Kraatz, H. B. *Chem. Commun.* **2008**, 502–504. (c) Moriuchi, T.; Nomoto, A.; Yoshida, K.; Ogawa, A.; Hirao, T. *J. Am. Chem. Soc.* **2001**, 123, 68–75. (d) Kuik, Å.; Skoda-Földes, R.; Jánosi, L.; Collar, L. *Synthesis* **2007**, 10, 1456–1458.
- (3) (a) Butler, I. R.; Quayle, S. C. *J. Organomet. Chem.* **1998**, 552, 63–68. (b) Okamura, T.; Sakauye, K.; Ueyama, N.; Nakamura, A. *Inorg. Chem.* **1998**, 37, 6731–6736. (c) Argyropoulos, N.; Coutouli-Artyropoulou, E. *J. Organomet. Chem.* **2002**, 654, 117–122. (d) Coutouli-Artyropoulou, E.; Sideris, C.; Kokkinidis, G. *J. Organomet. Chem.* **2006**, 691, 3909–3918. (e) Bertina, P. A.; Maedeb, T. *J. Tetrahedron Lett.* **2009**, 50, S409–S412.
- (4) (a) Molina, P.; Tárraga, A.; Caballero, A. *Eur. J. Inorg. Chem.* **2008**, 3401–3417. (b) Molina, P.; Tárraga, A.; Alfonso, M. *Eur. J. Org. Chem.* **2011**, 4505–4518.
- (5) Romero, T.; Caballero, A.; Tárraga, A.; Molina, P. *Org. Lett.* **2009**, 11, 3466–3469.
- (6) Sola, A.; Otón, F.; Espinosa, A.; Tárraga, A.; Molina, P. *Dalton Trans.* **2011**, 40, 12548–12559.
- (7) (a) Tárraga, A.; Otón, F.; Espinosa, A.; Velasco, M. D.; Molina, P.; Evans, D. *J. Chem. Commun.* **2004**, 458–459. (b) Otón, F.; Tárraga, A.; Molina, P. *Org. Lett.* **2006**, 8, 2107–2110. (c) Otón, F.; Espinosa, A.; Tárraga, A.; Ramírez de Arellano, C.; Molina, P. *Chem. Eur. J.* **2007**, 13, 5742–5752.
- (8) Dawson, W. R.; Windsor, M. W. *J. Phys. Chem.* **1968**, 72, 3251–3260.
- (9) Sheldrick, G. M. *SADABS: Program for Empirical Absorption Correction of Area Detector Data*; University of Göttingen, Göttingen, Germany, 1996.
- (10) Sheldrick, G. M. *SHELX-97: An Integrated System for Solving and Refining Crystal Structures from Diffraction Data*; University of Göttingen, Göttingen, Germany, 1996.
- (11) Neese, F. *ORCA-An ab Initio, Density Functional and Semiempirical Program Package, Version 2.8.0*; Universität Bonn, Bonn, Germany, 2010; <http://www.thch.uni-bonn.de/tc/orca/>. Tight convergence criteria for optimizations in ORCA: energy change 1.0×10^{-6} hartree; maximum gradient 1.0×10^{-4} hartree/ a_0 ; rms gradient 3.0×10^{-5} hartree/ a_0 ; maximum displacement $1.0 \times 10^{-3} a_0$; rms displacement $6.0 \times 10^{-4} a_0$.
- (12) (a) Becke, A. D. *J. Chem. Phys.* **1993**, 98, 5648–5652. (b) Lee, C. T.; Yang, W. T.; Parr, R. G. *Phys. Rev. B* **1988**, 37, 785–789.
- (13) Neese, F.; Wennmohs, F.; Hansen, A.; Becker, U. *Chem. Phys.* **2009**, 356, 98–109.
- (14) Weigend, F.; Ahlrichs, R. *Phys. Chem. Chem. Phys.* **2005**, 7, 3297–3305.
- (15) (a) Grimme, S. *J. Comput. Chem.* **2004**, 25, 1463–1476. (b) Grimme, S. *J. Comput. Chem.* **2006**, 27, 1787–1799.
- (16) Schäfer, A.; Huber, C.; Ahlrichs, R. *J. Chem. Phys.* **1994**, 100, 5829–5835; basis sets may be obtained from the Basis Set Exchange (BSE) software and the EMSL Basis Set Library: <https://bse.pnl.gov/bse/portal>. Feller, D. *J. Comput. Chem.* **1996**, 17, 1571–1586.
- (17) Wiberg, K. *Tetrahedron* **1968**, 24, 1083–1096.
- (18) (a) Mayer, I. *Chem. Phys. Lett.* **1983**, 97, 270–274. (b) Mayer, I. *Int. J. Quantum Chem.* **1984**, 26, 151–154. (c) Mayer, I. *Theor. Chim. Acta* **1985**, 67, 315–322. (d) Mayer, I. In *Modelling of Structure and Properties of Molecules*; Maksic, Z. B., Ed.; Wiley: New York, Chichester, Brisbane, Toronto, 1987. (e) Bridgeman, A. J.; Cavigliasso, G.; Ireland, L. R.; Rothery, J. *Dalton Trans.* **2001**, 2095–2108.
- (19) (a) Bader, R. F. W. In *Atoms in Molecules: A Quantum Theory*; Oxford University Press: Oxford, U.K., 1990. (b) Bader, R. F. W. *Chem. Rev.* **1991**, 91, 893–928. (c) Matta, C. F.; Boyd, R. J. In *The Quantum Theory of Atoms in Molecules*; Matta, C. F., Boyd, R. J., Eds.; Wiley-VCH: New York, 2007; pp 1–34.
- (20) (a) Biegler-König, F.; Schönbohm, J. *AIM2000 v. 2.0*; 2002; <http://www.aim2000.de/>. Biegler-König, F.; Schönbohm, J.; Bayles, D. *J. Comput. Chem.* **2001**, 22, 545–559. (b) Biegler-König, F.; Schönbohm, J. *J. Comput. Chem.* **2002**, 23, 1489–1494.
- (21) Frisch, M. J.; Trucks, G. W.; Schlegel, H. B.; Scuseria, G. E.; Robb, M. A.; Cheeseman, J. R.; Scalmani, G.; Barone, V.; Mennucci, B.; Petersson, G. A.; Nakatsuji, H.; Caricato, M.; Li, X.; Hratchian, H. P.; Izmaylov, A. F.; Bloino, J.; Zheng, G.; Sonnenberg, J. L.; Hada, M.; Ehara, M.; Toyota, K.; Fukuda, R.; Hasegawa, J.; Ishida, M.; Nakajima, T.; Honda, Y.; Kitao, O.; Nakai, H.; Vreven, T.; Montgomery, Jr., J. A.; Peralta, J. E.; Ogliaro, F.; Bearpark, M.; Heyd, J. J.; Brothers, E.; Kudin, K. N.; Staroverov, V. N.; Kobayashi, R.; Normand, J.; Ragahavachari, K.; Rendell, A.; Burant, J. C.; Iyengar, S. S.; Tomasi, J.; Cossi, M.; Rega, N.; Millam, N. J.; Klene, M.; Knox, J. E.; Cross, J. B.; Bakken, V.; Adamo, C.; Jaramillo, J.; Gomperts, R.; Stratmann, R. E.; Yazayev, O.; Austin, A. J.; Cammi, R.; Pomelli, C.; Ochterski, J. W.; Martin, R. L.; Morokuma, K.; Zakrzewski, V. G.; Voth, G. A.; Salvador, P.; Dannenberg, J. J.; Dapprich, S.; Daniels, A. D.; Farkas, Ö.; Foresman, J. B.; Ortiz, J. V.; Cioslowski, J.; Fox, D. J. *Gaussian 09, Revision A.02*; Gaussian, Inc., Wallingford, CT, 2009.
- (22) VMD-Visual Molecular Dynamics: Humphrey, W.; Dalke, A.; Schulten, K. *J. Mol. Graphics* **1996**, 14, 33–38, <http://www.ks.uiuc.edu/Research/vmd/>.
- (23) Mercury-visualization and analysis of crystal structures: Macrae, C. F.; Edgington, P. R.; McCabe, P.; Pidcock, E.; Shields, G. P.; Taylor, R.; Towler, M.; van de Streek, J. *J. Appl. Crystallogr.* **2006**, 39, 453–457.
- (24) (a) Rostovtsev, V.; Green, L. G.; Kokin, V. V.; Sharpless, K. B. *Angew. Chem., Int. Ed.* **2002**, 41, 2596–2599. (b) Tornoe, C. V.; Christensen, C.; Medal, M. *J. Org. Chem.* **2002**, 67, 3057–3064.
- (25) Siemeling, U.; Rother, D. *J. Organomet. Chem.* **2009**, 694, 1055–1058.
- (26) Li^+ , K^+ , Mg^{2+} , Ni^{2+} , Cd^{2+} , and Pb^{2+} were added as perchlorate salts and Na^+ , Ca^{2+} , Cu^{2+} , and Hg^{2+} as triflate salts. Zn^{2+} was used indistinctly as a perchlorate or triflate salt because the titration experiments gave rise to the same results. *Caution!* Metal perchlorate salts are potentially explosive under certain conditions. All due precautions should be taken while handling perchlorate salts.
- (27) The OSWV technique has been employed to obtain well-resolved potential information, while the individual redox processes are poorly resolved in the CV experiments, in which individual $E_{1/2}$ potentials cannot be easily or accurately extracted from these data: (a) Serr, B. R.; Andersen, K. A.; Elliot, C. M.; Anderson, O. P. *Inorg. Chem.* **1988**, 27, 4499–4504. (b) Richardson, D. E.; Taube, H. *Inorg. Chem.* **1981**, 20, 1278–1285.
- (28) *Specfit/32 Global Analysis System*; Spectrum Software Associates, 1999–2004; SpecSoft@compuserve.com
- (29) The criteria applied for reversibility was a separation of 60 mV between cathodic and anodic peaks, a ratio for the intensities of the cathodic and anodic currents I_c/I_a of 1.0, and no shift of the half-wave potentials with varying scan rates.
- (30) (a) Lloveras, V.; Caballero, A.; Tárraga, A.; Velasco, M. D.; Espinosa, A.; Wurst, K.; Evans, D. J.; Vidal-Gancedo, J.; Rovira, C.; Molina, P.; Veciana, J. *Eur. J. Inorg. Chem.* **2005**, 2436–2450. (b) Caballero, A.; García, R.; Espinosa, A.; Tárraga, A.; Molina, P. *J. Org. Chem.* **2007**, 72, 1161–1173. (c) Caballero, A.; Espinosa, A.; Tárraga, A.; Molina, P. *J. Org. Chem.* **2008**, 73, 5489–5497. (d) Martínez, R.; Zapata, F.; Caballero, A.; Espinosa, A.; Tárraga, A.; Molina, P. *Arkivoc* **2010**, iii, 124–144.
- (31) (a) Connolly, N. G.; Geiger, W. E. *Chem. Rev.* **1996**, 96, 877–910. (b) Caballero, A.; Espinosa, A.; Tárraga, A.; Molina, P. *J. Org. Chem.* **2008**, 73, 5489–5497. (c) Zapata, F.; Caballero, A.; Espinosa, A.; Tárraga, A.; Molina, P. *J. Org. Chem.* **2009**, 74, 4787–4796.
- (32) (a) Evans, A. J.; Watkins, S. E.; Craig, C.; Colbran, S. B. *Dalton Trans.* **2002**, 983–994. (b) Potts, K. T.; Keshavarz-K, M.; Tham, F. S.; Abrufa, H. D.; Arana, C. R. *Inorg. Chem.* **1993**, 32, 4422–4435. (c) Cui, X.; Carapuca, H. M.; Delgado, R.; Drew, M. G. B.; Felix, V. *Dalton Trans.* **2004**, 1743–1751. (d) Otón, F.; Tárraga, A.; Espinosa, A.; Velasco, M. D.; Molina, P. *Dalton Trans.* **2006**, 3685–3692. (e) Sato, M.; Katada, M.; Nakashima, S.; Sano, H. *J. Chem. Soc., Dalton Trans.* **1990**, 1979–1984. (f) Plenio, H.; Aberle, C.; Shihadeh, Y. A.; Lloris, J. M.; Martínez-Máñez, R.; Pardo, T.; Soto, J. *Chem. Eur. J.* **2001**, 7, 2848–2861.
- (33) (a) Marder, S. R.; Perry, J. W.; Tiemann, B. G. *Organometallics* **1991**, 10, 1896–1901. (b) Coe, B. J.; Jones, C. J.; McCleverty, J. A.;

- Bloor, D.; Cross, G. J. *J. Organomet. Chem.* **1994**, *464*, 225–232.
(c) Müller, T. J.; Netz, A.; Ansorge, M. *Organometallics* **1999**, *18*, 5066–5074. (d) Carr, J. D.; Coles, S. J.; Asan, M. B.; Hurthouse, M. B.; Malik, K. M. A.; Tucker, J. H. R. *J. Chem. Soc., Dalton Trans.* **1999**, 57–62.
- (34) (a) Geoffroy, G. L.; Wrighton, M. S. *Organometallic Photochemistry*; Academic Press: New York, 1979. (b) Gray, H. B.; Sohn, Y. S.; Hendrickson, N. *J. Am. Chem. Soc.* **1971**, *93*, 3603–3612.
- (35) (a) Barlow, S.; Bunting, H. E.; Ringham, C.; Green, J. C.; Bublitz, G. U.; Boxer, S. G.; Perry, J. W.; Marder, S. R. *J. Am. Chem. Soc.* **1999**, *121*, 3715–3723. (b) Southhard, G. E.; Curtis, M. D. *Organometallics* **2001**, *20*, 508–522. (c) Naka, K.; Uemura, T.; Chujo, Y. *Macromolecules* **2000**, *33*, 6965–6969.
- (36) Shortreed, M.; Kopelman, R.; Kuhn, M.; Hoyland, B. *Anal. Chem.* **1996**, *68*, 1414–1418.
- (37) Connors, K. A. *Binding Constants*; Wiley: New York, 1987.
- (38) Robin, M.; Day, P. *Adv. Inorg. Chem. Radiochem.* **1967**, *10*, 247–422.
- (39) CHEF is defined as I_{\max}/I_0 , where I_{\max} corresponds to the maximum emission intensity of the receptor–metal complex and I_0 is the maximum emission intensity of the free receptor.
- (40) Schaefer, A.; Horn, H.; Ahlrichs, R. *J. Chem. Phys.* **1992**, *97*, 2571–2577.
- (41) Shimonir-Livny, L.; Glusker, J. P.; Bock, C. W. *Inorg. Chem.* **1998**, *37*, 1853–1867.